Dark matter annihilation in the local group

Lidia Pieri*
Dept. of Physics, Università di Roma Tre, Rome, Italy
and INFN Roma Tre, Rome, Italy

Enzo Branchini
Dept. of Physics, Università di Roma Tre, Rome, Italy
(Received 10 July 2003; published 27 February 2004)

Under the hypothesis of a dark matter composed by supersymmetric particles such as neutralinos, we investigate the possibility that their annihilation in the halos of nearby galaxies could produce detectable fluxes of γ photons. Expected fluxes depend on several, poorly known quantities such as the density profiles of dark matter halos, the existence and prominence of central density cusps and the presence of a population of subhalos. We find that, for all reasonable choices of dark matter halo models, the intensity of the γ-ray flux from some of the nearest extragalactic objects, such as M31, is comparable to or higher than the diffuse galactic foreground. We show that next generation ground-based experiments could have the sensitivity to reveal such fluxes which could help us to unveil the nature of dark matter particles.

DOI: 10.1103/PhysRevD.69.043512 PACS number(s): 95.35.+d, 98.56.−p, 98.70.Rz

I. INTRODUCTION

The nature of the dark matter (DM) is a fundamental missing piece of the dark puzzle of the Universe, and represents one of the hottest challenges facing particle physics and cosmology today. The latest observational data [1] prefer a flat universe with a $\sim$23% mass fraction of DM, seeded with Gaussian, scale independent adiabatic perturbations. The bulk of DM is believed to be ''cold,'' i.e. composed by weakly interacting particles that were nonrelativistic at the epoch of decoupling. The most popular candidate for cold dark matter (CDM) is the lightest supersymmetric particle (LSP) which, in most supersymmetry breaking scenarios, is the neutralino χ. Neutralinos are spin-$\frac{1}{2}$ Majorana fermions, linear combinations of the neutral gauge bosons and neutral Higgs doublet spartners, $\chi^0 = a\tilde{B} + b\tilde{W}_3 + c\tilde{H}_1^0 + d\tilde{H}_2^0$. In the popular supergravity (SUGRA) or SUGRA-like models, where gaugino universality is required, its mass is constrained by accelerator searches and by theoretical considerations of thermal freeze-out to lie in the range 50 GeV $\lesssim m_\chi \lesssim$ 10 TeV [2,3]. Neutralinos decouple at a temperature that is roughly $m_\chi/20$; hence, they behave like CDM. If R parity is conserved, neutralinos are stable and can change their cosmological abundance only through annihilation, which implies that the resulting production of detectable matter, antimatter, neutrinos and photons is enhanced in high density regions like the center of virialized DM halos. At low energies, direct detection terrestrial experiments are being performed to measure the energy deposited by elastic neutralino-nucleon scattering [4,5]. In addition to direct searches, indirect detection of DM through its annihilation products can be implemented [6,7], which are necessary for energies greater than 250 GeV. Most indirect searches rely on detection of antimatter [8,9] and γ rays produced in the Milky Way halo [10–12] or in Galactic substructures [13,14]; the possibility of looking at extragalactic sources has also been suggested [13,15–20]. Unfortunately, our partial knowledge of those astrophysical processes that govern the assembly of DM concentrations did not allow us to make firm predictions on DM detectability. In particular, the central structure of the DM halos and the prominence of small scale structures within the smooth DM halo are far from being well determined. The purpose of this work is to explore the possibility of extending DM searches to extragalactic sources in our local group of galaxies (LG) and to make robust predictions about their actual detectability with ground-based experiments once model uncertainties are taken into account. Supersymmetric LSP are not the only particles which can produce annihilation signals (e.g. [21]), yet in this work we focus on the contribution of neutralinos only.

The outline of the paper is as follows. In Sec. II we discuss the theoretical framework and present the predictions from the smooth halo models. In Secs. III and IV we show how predictions change when the presence of Supermassive Black Holes (SMBH) and that of a population of subgalactic halos are taken into account. Section V deals with the actual detectability of LG sources and Galactic subhalos by ground-based detectors. Our conclusions are presented in Sec. VI.

II. THEORETICAL FRAMEWORK

In a phenomenological approach which considers the LSP as a DM candidate, the expected photon flux from neutralino annihilation is given by

$$\frac{d\Phi_\gamma(E)}{dE_\gamma} = \left[\sum_{V=\gamma,Z} N_{V\gamma} b_{V\gamma} \delta\left(E_\gamma - m_\chi \left(1 - \frac{m_V^2}{4m_\chi^2} \right) \right) + \sum_F \frac{dN_\gamma}{dE_\gamma} b_F \right] \frac{\langle \sigma_a v \rangle}{2m_\chi^2} \int_0^{r_{max}} \frac{\rho_\chi^2(r)}{D^2} r^2 dr. \quad (1)$$

*Electronic address: pieri@fis.uniroma3.it

In this formula, the dependence of the flux on particle physics inputs and on cosmological inputs is factorized.

Particle physics. The first sum in brackets represents a γ line, i.e. the 1-loop mediated process $\chi\chi\rightarrow\gamma\gamma$ or $\chi\chi\rightarrow Z\gamma$. Since neutralinos move at Galactic speed [22], their annihilation occurs at rest and the outgoing photons carry an energy equal ($\gamma\gamma$ final state) or very close ($Z\gamma$ final state) to the neutralino mass. For the corresponding γ lines we have $N_{\gamma\gamma}=2$ and $N_{Z\gamma}=1$ monochromatic final state photons. Branching ratios $b_{Z\gamma}\sim b_{\gamma\gamma}\sim 10^{-3}$ imply that the photon flux is dominated by the continuum emission rather than by the γ lines. The continuum emission is given by the second sum of Eq. (1) running over all the tree-level final states. At the tree level, neutralinos annihilate into fermions, gauge bosons, Higgs particles and gluons. Decay and/or hadronization in π^0 give a continuum spectrum of γ photons emerging from the π^0 decay. Depending on the annihilation channel, the continuum differential energy spectrum can be parametrized as $dN_\gamma/dx=ax^{-1.5}e^{-bx}$, where $x=E_\gamma/m_\chi$, $a\sim O(1)$ and $b\sim O(10)$. These spectra have been calculated in [12] using a PYTHIA Monte Carlo simulation. Branching ratio b_F calculations for each process involved in the sum and the evaluation of the total annihilation cross section $\langle\sigma_a v\rangle$ depend on the assumed supersymmetric model. Here we consider as a unique annihilation channel the one into W bosons, $\chi\chi\rightarrow W^+W^-$, with parameters $a=0.73$ and $b=7.76$ in the above mentioned dN_γ/dx formula. We also use the constraint to the value of the thermally averaged annihilation crosssection $\langle\sigma_a v\rangle$ given by the neutralino number density at the freeze-out epoch [3]:

$$\Omega_\chi h^2\sim\frac{3\times10^{-27}\ \mathrm{cm^3\,s^{-1}}}{\langle\sigma_a v\rangle}, \tag{2}$$

where h is the Hubble constant, H, in units of 100 km s^{-1} Mpc^{-1} and Ω_χ is the average density of neutralinos in units of critical density, $\rho_c=3H^2/8\pi G$.

Unless otherwise specified, throughout the paper we consider neutralinos with a mass of 1 TeV and cross section $\langle\sigma_a v\rangle=2\times10^{-26}$ cm^{-3} s^{-1}.

Cosmology. The last term in Eq. (1) describes the geometry of the problem and assumes that the DM is concentrated in a single, spherical DM halo of radius r_{max} and density profile $\rho_\chi(r)$ located at distance D from the observer. The integral can be easily generalized to any DM distribution once the DM density along the line of sight, $\rho_\chi(r)$, is specified.

An accurate evaluation of this integral should account for the fact that DM halos are triaxial rather than spherical objects [23]. Deviations from sphericity do not change appreciably the γ-ray flux from LG objects within the typical acceptance angle of the detectors ($0.1°-1°$) and would only enhance the Galactic flux by a modest 15% [24] and thus will not be considered here. The shapes of the halo density profiles are poorly constrained by observations, especially near the center. Indeed, recent measurements of the dwarf galaxy rotation curves, as well as of the intracluster medium and of the gravitational lensing, could not discriminate between dark halos with constant density core and r^{-1} cusps [25]. Similarly, analytical arguments did not yet lead to a definitive, unique prediction [26–28].

The most stringent constraints on the shape of DM halos are currently obtained from N-body simulations. Although the resolution in numerical experiments is still an issue [29], advances in numerical techniques have allowed us to discover that DM halos have universal density shapes $\rho_\chi(r)\sim\rho_s(r/r_s)^{-\alpha}$. While singular isothermal halos characterized by a steep r^{-2} cusp are ruled out, current numerical experiments do not allow us to discriminate among the Moore profile [30] characterized by $\alpha=1.5$ and the shallower NFW profile [31] with $\alpha=1$ (or slightly shallower ones [24]). In this paper we assume that the actual shape of the DM density profiles is bracketed by the Moore and the NFW models and thus we can obtain a fair estimate of current model uncertainties by considering both of them in our analysis. Both models have central cusps where the neutralino annihilation rate is greatly enhanced. The scale radius, r_s, and the scale density, ρ_s, can be fixed by observations (the virial mass of the halo or its rotation velocity) and theoretical considerations that allow us to determine the concentration parameter $c=r_{vir}/r_s$ (where the virial radius, r_{vir}, is defined as the radius within which the halo average density is $200\rho_c$).

Since the largest γ-ray fluxes are expected from nearby objects, we have considered only the 44 nearest LG galaxies and their parent halos. Table I lists the masses, positions (from [32]) and virial radii of the galaxies which are more relevant for our analysis, along with their scale radii and scale densities computed assuming a Moore profile. Their concentration parameters, c_{NFW} and $c_{Moore}=0.64\,c_{NFW}$, have been computed according to [33] assuming CDM power spectrum with a shape parameter $\Gamma=0.2$, normalized to $\sigma_8=0.9$. In our analysis we have also included the giant elliptical galaxy M87 at the center of the Virgo cluster whose predicted annihilation flux was already computed by [19]. The mass, distance and the virial radius of M87, listed in Table I, are taken from [34].

Since the intensity of the γ-ray flux is proportional to ρ_χ^2, great attention must be paid in modeling the central region of the halo. The fact that the Moore model predicts a divergent flux from the halo center implies that there must exist a minimum radius, r_{min}, within which the self-annihilation rate $t_l\sim[\langle\sigma_a v\rangle n_\chi(r_{min})]^{-1}$ equals the dynamical time $t_{dyn}\sim(G\overline{\rho_\chi})^{-1/2}$, where $\overline{\rho_\chi}$ is the mean halo density within r_{min} [35]. We have used this prescription to determine r_{min} for all our 44 halos and model their DM distribution with a NFW or a Moore profile with a small constant core $\rho_\chi(r_{min})$. The resulting profiles are

$$\rho_\chi(r)=\frac{\rho_s^{nfw}}{\left(\frac{r}{r_s^{nfw}}\right)\left(1+\frac{r}{r_s^{nfw}}\right)^2},\quad r>r_{min}$$

$$\rho_\chi(r)=\rho_\chi^{nfw}(r_{min}),\quad r\leqslant r_{min} \tag{3}$$

for the NFW case, and

TABLE I. Input parameters for the γ-ray flux prediction are shown for our Galaxy, M87 and for the LG galaxies brighter than the Galactic foreground. Masses and distances are taken from [32]. Virial radii were calculated following the prescription given in the text. Scale radii and scale densities were computed assuming a Moore profile.

Galaxy name	mass ($M_\odot$)	distance (kpc)	r_{vir} (kpc)	r_s^{moore} (kpc)	ρ_s^{moore} ($M_\odot$ kpc^{-3})
MW	1.0×10^{12}	8.5	205	34.5	1.1×10^{6}
Sagittarius	9.4×10^{8}	24	20	2.5	2.3×10^{6}
SMC	2.5×10^{9}	58	28	3.6	2.1×10^{6}
LMC	1.4×10^{10}	49	49	6.8	1.8×10^{6}
M31	2.0×10^{12}	770	258	47.3	8.6×10^{5}
M33	4.0×10^{10}	840	70	10.6	1.6×10^{6}
M87	4.2×10^{14}	1.5×10^{4}	1.55×10^{3}	461	2.6×10^{5}

$$\rho_\chi(r)=\frac{\rho_s^{moore}}{\left(\frac{r}{r_s^{moore}}\right)^{1.5}\left[1+\left(\frac{r}{r_s^{moore}}\right)^{1.5}\right]},\quad r>r_{min}$$

$$\rho_\chi(r)=\rho_\chi^{moore}(r_{min}),\quad r\leqslant r_{min} \tag{4}$$

for the Moore case.

Figure 1 shows an Aitoff projection of the angular position of these LG galaxies in Galactic coordinates. The size of each point is proportional to the γ-ray flux from Moore models, measured within a viewing angle of 1°.

As shown by [13], high energy γ-ray flux from nearby extragalactic halos with a Moore density profile can be larger than the γ-ray foreground produced by neutralino annihilation in our Galaxy. This is not an entirely trivial point as distant extragalactic objects are not resolved within the typical 1° angular resolution of the γ-ray detectors. To check whether our conclusions still hold for shallower density profiles, we have computed the γ-ray flux using both Moore and NFW models for our LG halos and compared it to the Galactic foreground. In this work all fluxes are computed above 100 GeV within an angle $\Delta\Omega=10^{-3}$ sr. Note that none of the particle physics assumptions affect the ratio between Galactic and extragalactic fluxes that we will focus on.

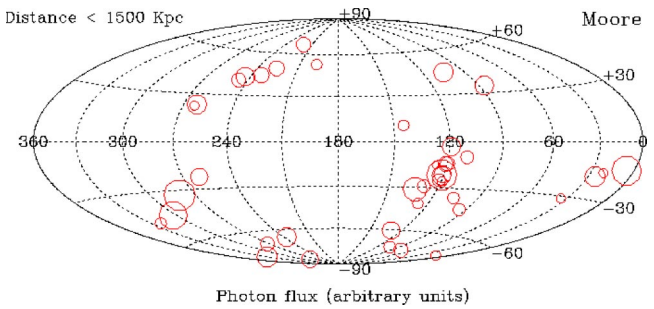

FIG. 1. Aitoff projection of the 44 nearest LG galaxies in Galactic coordinates. The size of each symbol is scaled to the γ-ray flux emitted by a host DM halo with a Moore profile within a viewing angle of 1° from the halo center.

Figure 2 shows the smooth γ-ray Galactic foreground for a Moore (continuous line) and a NFW (dotted line) profile as a function of ψ, the angle from the Galactic Center (GC). Filled triangles represent the γ fluxes from those LG galaxies which are brighter than the Galactic foreground and from M87, assuming a Moore profile. The fluxes from the Small and Large Magellanic Clouds (SMC, LMC), M31 and, to a lesser extent, M87 are above the Galactic level. In some cases, such as, M33 and Sagittarius, extragalactic and Galactic contributions are comparable. Similar considerations are valid for the case of a NFW profile (filled dots), despite the significant reduction of the extragalactic fluxes that cause M33 and Sagittarius to be dimmer than the Galactic foreground.

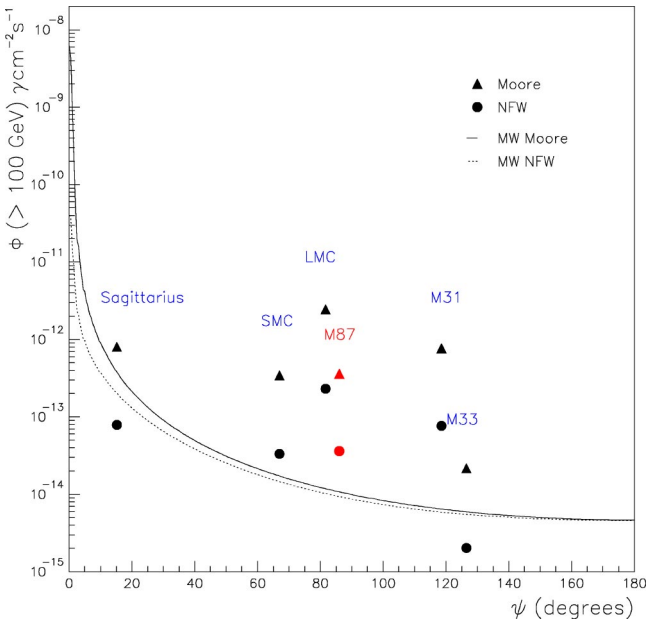

FIG. 2. Integrated γ-ray flux within $\Delta\Omega=10^{-3}$ sr as a function of the angular distance from the GC. Filled triangles and filled dots represent the fluxes from brightest extragalactic objects predicted assuming a Moore and a NFW profile, respectively. The continuous and the dashed curves show the predicted Galactic foreground for the two model density profiles.

III. BLACK HOLES, CUSPS AND CORES

The previous results do not account for those astrophysical processes which may modify the density near the halo center, like the presence of a central SMBH. The effect of a SMBH on the central shape of a DM profile is, in fact, rather controversial. The adiabatic growth of a SMBH of mass $M_\bullet$ at the center of a DM halo would steep the slope of the density profile to $\rho_{halo} \propto r^{-\gamma}$, $2.2 < \gamma < 2.5$ within a radius $r_h \equiv G M_\bullet / \sigma_v^2$, where σ_v is the 1D RMS velocity dispersion of the DM particles [36]. As a consequence, the expected γ-ray emission would be larger in galaxies hosting SMBHs. However, when one takes into account dynamical processes such as merger and orbital decay of an off-centered SMBH [37], this central ''spike'' disappears or is greatly weakened. Moreover, in a CDM cosmology the assembly of black holes at the center of galaxies is the end-product of the hierarchical build up of their parent halos. In this scenario pregalactic black holes become incorporated through series of mergers into larger and larger halos, sink to the center owing to dynamical friction, form a binary system [38] and eventually coalesce [39] with the emission of gravitational waves. The process of formation and decay of black hole binaries transfers angular momentum to the DM particles, ejects them via a gravitational slingshot effect and thus decreases the mass density around the binary [40,41]. The net result is either a constant density core [42] or a shallower DM density profile $\rho_\chi \sim r^{-0.5}$ within a radius $r_{cut} = 10 - 100$ pc, with a consequent decrease of the neutralinos annihilation rate [43].

Observations indicate that SMBHs are only found in large galaxies. Indeed, among the LG galaxies only the Milky Way and M31 harbor a SMBH, while a possible black hole in M33 would have a mass smaller than $3000 M_\odot$ [44]. Assuming that the presence of a SMBH creates a constant density core of similar size in both the dark and stellar components, we expect a small core $r_{cut} = 0.38$ pc in our Galaxy [45] and one of $r_{cut} \sim 10$ pc at the center of M31 [42]. As a consequence, the SMBH phenomenon would only decrease the expected γ-ray flux from M31 by a factor of 3, still well above the Galactic foreground. In fact, our predictions do not change much even under the somewhat extreme hypothesis that all DM halos hosting LG galaxies have a constant density core of size 10–100 pc. Indeed, when repeating our calculation using both NFW and Moore profiles truncated at 10 and 100 pc we do find that the DM depletion near the halo center causes a significant decrease of the γ-ray flux which, however, does not prevent a few objects from shinning prominently above the Galactic foreground. Results are shown in Fig. 3 in which the fluxes from Moore DM halos (filled triangles), already shown in Fig. 2, are compared to the cases of Moore profiles truncated at $r_{cut} = 10$ pc (filled squares) and at $r_{cut} = 100$ pc (filled circles).

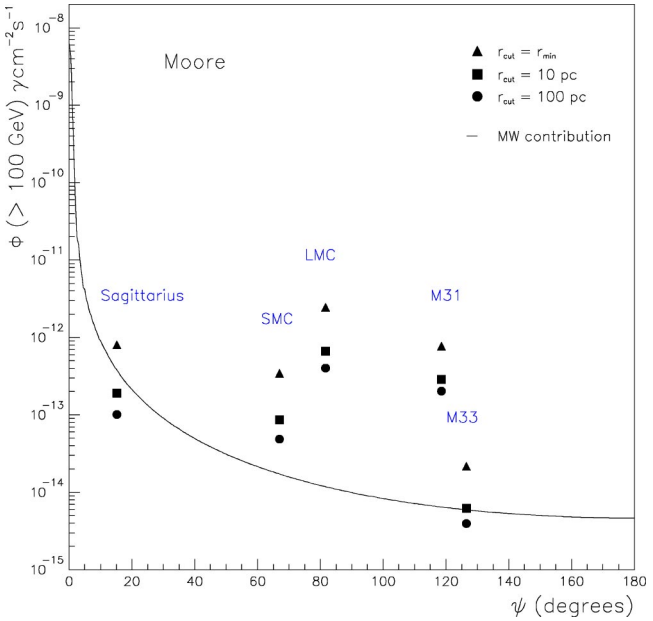

FIG. 3. Integrated γ-ray flux from the brightest LG members computed assuming a standard Moore profile (filled triangles) and a Moore profile truncated at 10 pc and 100 pc (filled squares and filled dots, respectively). The continuous line shows the expected Galactic annihilation foreground.

IV. HALO SUBSTRUCTURES

Despite its remarkable success in explaining the large majority of current observations, the excess power on small scales in the ΛCDM concordance model has led to what is sometimes called *the CDM crisis*. One aspect of this problem is the presence of a density spike at the center of DM halos, that is difficult to reconcile with the observed rotation curves of nearby dwarf galaxies [25]. A second aspect is related to the measured zero-point of the Tully-Fisher relation for spiral galaxies [46], which is smaller than the CDM-predicted one. Whether these discrepancies are genuine or artifacts arising from observational biases (e.g. beam-smearing effect in determining the rotation velocities of dwarf galaxies) or numerical effects (e.g. limited resolution in CDM N-body experiments) is still a matter of debate. A second problem, also related to the excess small-scale power in the CDM model, is the wealth of subgalactic, virialized halos that do not appear to have an observational counterpart (the so called *satellite catastrophe* [30]). Numerical simulations have indeed shown that a CDM halo of the size of our Galaxy should have about 50 satellites with circular velocities $v_{circ} > 20$ km s^{-1} instead of the dozen observed ones [47]. Due to the hierarchical nature of the clustering process in a CDM scenario, the mismatch is also found on larger systems of the size of the LG. Model predictions for halos with $v_{circ} > 35$ km s^{-1} might be reconciled with observations by delaying the formation epoch of DM halos or by computing their peak rotation velocity with different techniques [48]. For lighter halos, however, the lack of a luminous counterparts could be either ascribed to astrophysical processes (supernovae explosion, stellar feedback, gas heating by ionizing radiation of cosmic origin) that suppress star formation or to a genuine disruption of the DM subhalos by gravitational tides within their massive host. Finally, invoking the warm dark matter scenario decreases the small scale power and thus avoids the satellite catastrophe but would postpone the reionization of the Universe to an epoch too late to be con-

sistent with the recent WMAP observations of the cosmic microwave background [49].

Here we account for the presence of a population of DM subhalos and investigate their effect on the neutralino annihilation signal. Model predictions and related uncertainties are obtained using both numerical experiments and theoretical arguments.

Large N-body simulations [30,50] have shown that DM halos host a population of subhalos characterized by a distribution function giving the probability of finding a subhalo of mass m at distance r from the halo center, that can be modeled as follows [51]:

$$n_{sh}(r,m)=A\left(\frac{m}{m_H}\right)^{-1.9}\left[1+\left(\frac{r}{r_c^{sh}}\right)^2\right]^{-1.5} \tag{5}$$

where r_c^{sh} is the core radius of the subhalos distribution, m_H is the mass of the parent halo and A is a constant set to obtain 500 subhalos of mass $\geqslant 10^8 M_\odot$ in a halo with $m_H=2\times10^{12}M_\odot$ [50]. The annihilation rate within subhalos may contribute significantly to the total γ-ray flux. According to [13,14] the γ-ray Galactic foreground can be enhanced by over two orders of magnitude by the presence of a population of subhalos, an effect that may also help to explain the γ-ray flux excess found in EGRET data [52]. To account for this effect, we have populated all the halos of our LG galaxies including our own with a population of subhalos according to the distribution function (5) and computed their contribution to the γ-ray annihilation flux. For each subhalo we use the same density profiles as its massive host. Current N-body simulations do not allow us to model Eq. (5) very precisely. In particular, the mass clumped in subhalos, m_{cl}, and the value of r_c^{sh} are poorly constrained. To account for these model uncertainties we have generated several different subhalos distributions that explore the edges of the parameter space $[m_{cl},r_c^{sh}]$. Following [51] we have set m_{cl} equal to 10% and 20% of the total DM halo's mass, m_H, and the core radius, r_c^{sh}, to be 5% and 30% of the parent halo virial radius, r_{vir}^H. Subhalos were generated in a mass range $[m_{min}, 0.1\ m_H]$ and within a distance r_{vir}^H from the halo center. We set $m_{min}=10^6M_\odot$ for Galactic halos and $m_{min}=10^7M_\odot$ for the extragalactic ones since the slope of the subhalo mass distribution, Eq. (5), is shallow enough to ensure that for a fixed value of m_{cl} the contribution to the total γ-ray flux from halos with masses smaller than m_{min} becomes negligible [14,24].

Very high resolution N-body experiments show that in a CDM scenario a large fraction of the subhalo population survives the complete tidal disruption [23]. However, these subhalos are tidally stripped of a fraction of their mass originating debris streams and possibly changing their original profile at all radii, thus lowering the annihilation luminosity of the accreted systems [24,48,53]. Because of their finite resolution, the N-body experiments used to model Eq. (5) underestimate the role of these tidal fields and therefore do not allow a reliable sampling of the low mass tail of the subhalo distribution at small r. To better account for gravitational tides we follow [48] and use the "tidal approximation," i.e. we assume that all the mass beyond the subhalo tidal radius, r_{tid}, is lost in a single orbit without affecting its central density profile. The tidal radius is defined as the distance from the subhalo center at which the tidal forces of the host potential equal the self-gravity of the subhalo. In the Roche limit,

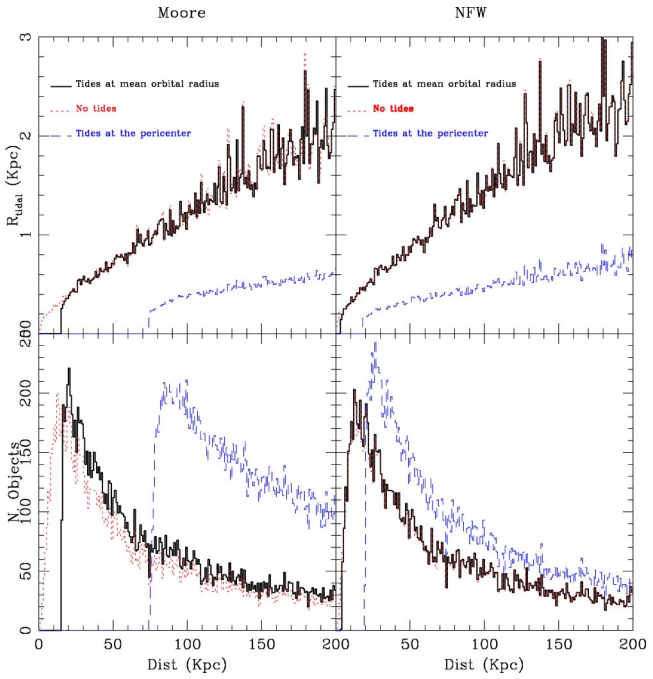

FIG. 4. Number of Galactic halos (bottom) and their average tidal radius (top) as a function of the Galactic radius for a Moore (left) and NFW (right) density profile. Short-dashed histogram: no tidal stripping allowed. Continuous line: tidal radius computed at the mean orbital radius. Long dashed: tidal radius computed at the pericenter of the subhalo orbit. In all cases shown $m_{cl}=20\%\ m_H$ and $r_c^{sh}=0.05\ r_{vir}^H$.

$$r_{tid}(r)=\left(\frac{m}{2m_H(<r)}\right)^{1/3}r, \tag{6}$$

where r is the distance from the halo center. We truncate all subhalos at their tidal radii and discard those with $r_{tid}<r_s$, for which the binding energy is positive and the system is dispersed by tides. Even in this case, we estimate the model uncertainties by considering three different cases: no tidal stripping, tidal radius computed at the mean orbital radius and tidal radius computed at the pericenter of the orbit (which is typically 1/5 of the mean orbital radius).

The short-dashed histograms in the two bottom panels of Fig. 4 show the radial distribution of all Galactic subhalos with $M>10^6M_\odot$, distributed according to Eq. (5) in which $m_{cl}=20\%\ m_H$ and $r_c^{sh}=5\%\ r_{vir}^H$ for both a Moore (left) and a NFW (right) density profile. Including the tidal stripping effect destroys all subhalos near the Galactic Center and modifies their radial distribution. The effect is larger for the Moore model (which is less concentrated than the NFW profile) and increases with the strength of the tidal field (i.e. when tides are computed at the pericenter of the orbit, long-

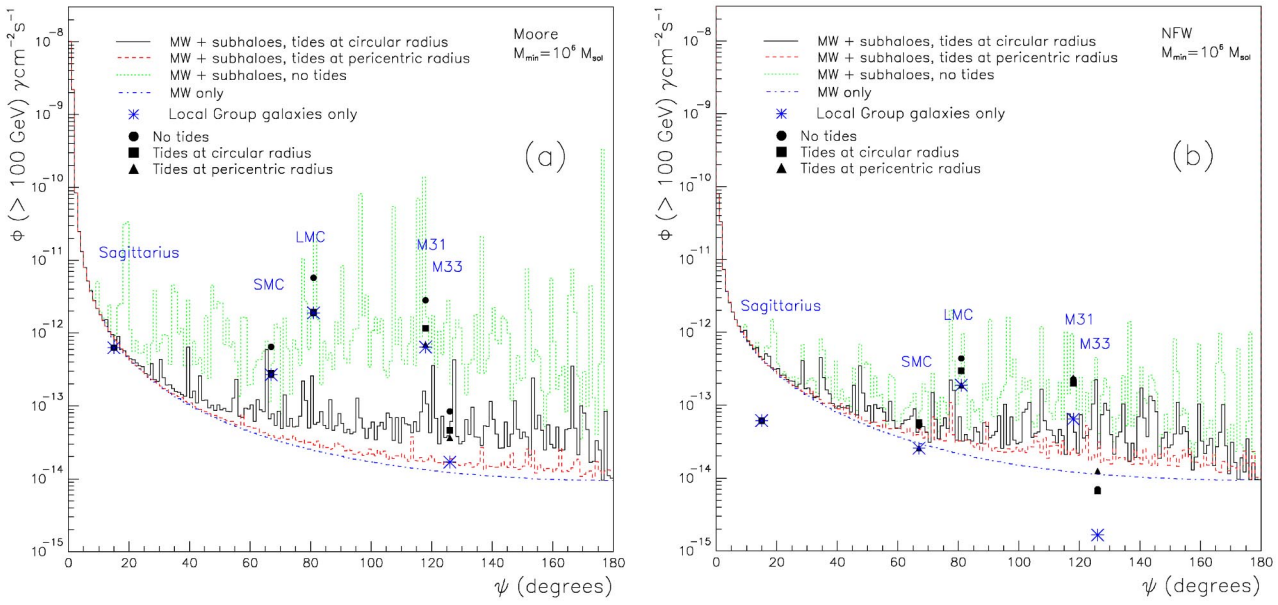

FIG. 5. Integrated γ-ray flux within $\Delta\Omega=10^{-3}$ sr for Moore (a) and NFW (b) DM halos populated with subhalos. Galactic (histograms) and extragalactic (symbols) fluxes are shown for the different subhalo populations described in the text.

dashed histogram). The two top panels show the average tidal radius, r_{tid} of the subhalo population that survive, tidal stripping.

The effect of subhalos on the emitted annihilation flux is shown in Fig. 5(a) for the case of a Moore profile and in Fig. 5(b) for a NFW profile. The histogram drawn with a dotted line shows the diffuse γ-ray flux obtained by adding the contribution to the smooth Galactic emission of a subhalo population distributed according to Eq. (5) in which $m_{cl}=20\%\ m_H$ and $r_c^{sh}=5\%\ r_{vir}^H$. Filled dots show the flux from the most prominent external objects, computed by adding together the halo flux to that of all their subhalos within 1° from the center and by neglecting gravitational tides. The presence of subhalos dramatically boosts up the level of the Galactic foreground (dot-dashed curve) by a factor 10–100, depending on the halo profile, while increasing the flux from extragalactic sources by a more modest factor 2–5. As a consequence, the Galactic foreground becomes dominated by the local subhalo emission, resulting in the irregular γ-ray Galactic brightness profiles that outshine all extragalactic objects but M31 and the LMC.

These results, which are consistent with those of [13,14], change significantly when tidal fields are accounted for. The net effect that is more apparent for a Moore density profile, is that of decreasing significantly the Galactic γ-ray foreground, as shown by the histogram drawn with a continuous line in Figs. 5(a) and 5(b). The flux from extragalactic objects (filled squares) is comparatively less affected by tidal effects and in some cases may actually be enhanced when the chance of bright foreground extragalactic subhalos becomes non-negligible. As a result, taking into account the tidal stripping effects increases the prominence of extragalactic sources over the Galactic foreground. If one further accounts for the eccentricity of the subhalo orbits and assumes tidal stripping occurs at their pericenter, then the Galactic γ-ray foreground (dashed histogram) and the flux from extragalactic objects (filled triangles) further decrease to a level similar to that of Fig. 2.

To better quantify the uncertainties in modeling the subhalo population we list in Table II the fractional variation of the γ-ray flux from the extragalactic sources when varying the model parameters. The quantity displayed is $\delta\Phi=(\Phi^{sh}-\Phi^0)/\Phi^0$, where Φ^0 is the flux from a smooth profile while the flux Φ^{sh} also accounts for the subhalo population. We have focused on the two brightest LG objects, M31 and the LMC. It is worth noticing that, due to their different dis-

TABLE II. The effect of including subhalos on the γ-ray flux from LMC and M31 in different halo models. Each entry specifies the fractional flux variation with respect to the smooth halo model. The choice of parameters is encoded in each model label as specified in the text.

	$\delta\Phi$					
Galaxy	0510dd	0520dd	3010dd	3020dd	0520d0	0520d5
LMC (Moore)	−0.12	−0.21	−0.12	−0.21	+1.35	−0.22
LMC (NFW)	−0.07	−0.18	−0.09	−0.18	+0.90	−0.18
M31 (Moore)	+0.25	+0.52	+0.03	+0.03	+2.69	−0.10
M31 (NFW)	+0.78	+1.59	+0.02	+0.05	+1.93	+2.09

tances from our Galaxy, while the flux from M31 is produced in the central 16–36 Kpc (depending on the model profile), the LMC flux is produced in a much smaller region of radius 1–1.4 Kpc. The various models explored are listed in Table II and are characterized by a label in which the first two digits indicate the extent of the core radius of the subhalo distribution (e.g. 30 means $r_c^{sh}=30\%\ r_{vir}^H$), the subsequent two digits characterize the mass clumped in subhalos (e.g. 20 for $m_{cl}=20\%\ m_H$) and the last two letters indicate the model tidal field ($d0$=no tidal effects, dd=tidal radius computed at the mean orbital radius, $d5$=tidal radius computed at the pericenter).

In all *dd* models considered, the flux from M31 is increased by the presence of subhalos while the flux from LMC decreases. This discrepancy reflects the different effect of the tidal field that, as we have seen, disrupts all the subhalos near the halo center and thus decreases the flux from the nearby LMC, while the flux from M31, which is produced in a broader region, receives a significant contribution from the nearby, foreground subhalos in M31. Varying m_{cl} in the allowed range does not change the fluxes appreciably, while increasing the core radius of the subhalo distribution decreases the M31 flux significantly but does not change significantly the flux received from the nearer LMC. Finally, neglecting the tidal field ($d0$ model) has the rather obvious effect of increasing the flux from both extragalactic objects. Enhancing the tidal disruption effect ($d5$ model) generally decrease the annihilation flux, apart from the case of M31-NFW, in which the flux is enhanced by the combined effect of the halo distance and the large DM concentration.

V. DETECTABILITY

In this section we explore the actual detectability of the γ-ray fluxes from both the extragalactic sources and the Galactic foreground.

Satellite borne experiments, such as GLAST [54], have very small effective areas at energies >250 GeV and thus are inefficient in revealing high energy photons from neutralino annihilation. The need for larger collecting areas can only be met by those ground-based experiments designed to detect the products of generic atmospheric showers. These detectors were not originally meant to explore exotic physics, yet recent advances in technology have allowed them to reach unprecedented high sensitivities and they can now be used to detect high energy photons from neutralino annihilation.

Čerenkov detectors. Electrons generated in showers emit Čerenkov light during their passage through the atmosphere. It reaches the ground in the form of a $\sim$100 meters wide light pool. Čerenkov detectors have good angular and energetic resolution, operate with a duty cycle of about 10% and have a very good hadronic background rejection. Their small angle of view ($\sim 5°$) makes them suitable for the observations of point sources like LG galaxies. Currently operating Čerenkov telescopes such as WHIPPLE [55] and HEGRA [56] do not have enough sensitivity to detect faint extragalactic sources. Planned Active Čerenkov Telescopes (ACT) such as HESS [57], MAGIC [58] and VERITAS [59] with their lower energy threshold ($\sim$50 GeV) and greater sensitivities make them suitable for our purposes.

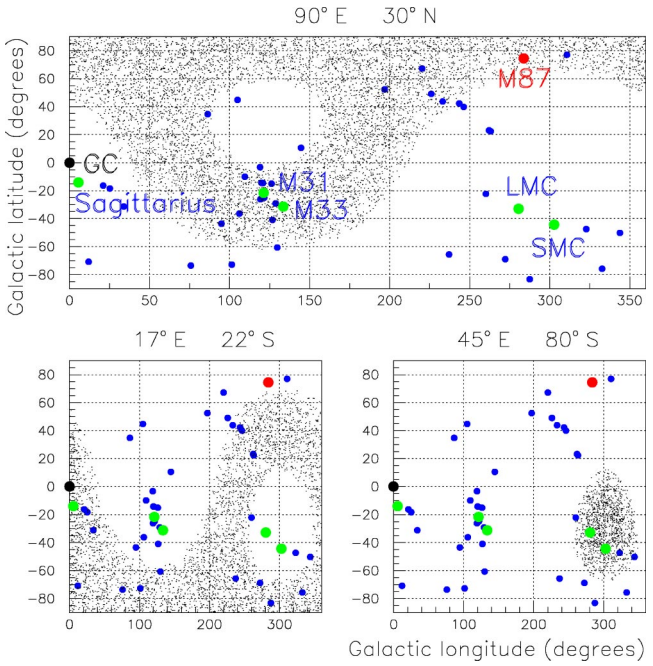

FIG. 6. Angular positions of our 44 LG galaxies (filled dots) inclusive of M87 and the GC in galactic coordinates. Shaded regions have zenith angles smaller than 30° at the ARGO site (upper panel), HESS site (lower left) and a hypothetical Antarctic site (lower right). Terrestrial longitude and latitude of each site are indicated above each panel.

Large field of view arrays. Unconventional air shower arrays at energies $<$TeV constitute viable alternative to Čerenkov telescopes. Unlike standard air shower arrays, these detectors can reconstruct lower energy showers by dense sampling of the shower particles. This can be achieved by operating the detector at very high altitude in order to approach the maximum size development of low energy showers and by using a full coverage layer of counters. Operating large field of view arrays like ARGO [60] and MILAGRO [61] have worse angular resolution and background rejection than ACT detectors, but are able to explore the whole sky with a duty cycle of about 100%.

Due to the complementarity of ACTs and large field of view arrays, we explore and compare the capabilities of these detectors to reveal the γ-ray flux from neutralino annihilation in extragalactic objects [62]. All analyses, including our own, have shown that the best place to look for DM annihilation signals is the GC, and indeed presently available and future detectors should be able to detect such γ-ray emission. However, most of them are (or will be) located in the Northern Hemisphere where the GC can only be seen for short periods and at uncomfortably large zenith angles. In Fig. 6 the angular positions of our extragalactic objects (filled dots) are shown in Galactic coordinates, superimposed to the areas that can be seen with a zenith angle smaller than 30° from various experimental sites (shaded areas). In the following we estimate the detectability of γ-ray fluxes from either external LG galaxies or subhalos within our Galaxy.

A. Detectability of external galaxies

In the following we will focus on the detectability of M31 since it is the extragalactic object with the largest γ-ray flux visible from the Northern hemisphere.

The detectability of the continuum flux from M31 is computed by comparing the number of γ events expected from this source to the fluctuations of background events. This ratio, which we call σ in the following, is given by

$$\frac{n_\gamma}{\sqrt{n_{bkg}}} = \frac{\sqrt{T_\delta}\epsilon_{\Delta\Omega}}{\sqrt{\Delta\Omega}} \frac{\int A_\gamma^{eff}(E,\theta)\frac{\phi_\gamma^{DM}}{dE}dEd\theta}{\sqrt{\int\int \sum_{bck} A_{bck}^{eff}(E,\theta)\frac{d\phi_{bck}}{dE}dEd\theta}}, \tag{7}$$

where T_δ is the time during which the source is seen with zenith angle $\theta \leqslant 30°$ and $\epsilon_{\Delta\Omega}=0.7$ is the fraction of signal events within the optimal solid angle $\Delta\Omega$ corresponding to the angular resolution of the instrument. The effective detection areas A^{eff} for electromagnetic and hadronic induced showers are defined as the detection efficiency times the geometrical detection area. For the case of a large field of view array we have considered $A^{eff}=10^2$–10^3 m^2, depending on the γ-photon energy, while for a Cerenkov apparatus we have assumed a conservative effective area of 10^4 m^2. Note that while the latter can be increased by adding together more Cerenkov telescopes, the former is intrinsically limited by the number of hits reaching the ground and cannot be much greater than our fiducial value. Finally we have assumed an angular resolution $\phi=1°$ and hadron-photon identification efficiencies of $\epsilon=75\%$ for the case of a large field of view array and $\phi=0.1°$ and $\epsilon=99\%$ for the Cerenkov apparatus. These values are appropriate for the energy range of interest.

Backgrounds. In our analysis the M31 flux is much smaller than electron, hadron and diffuse γ-ray backgrounds that must then be taken into account. We have considered the following values for the background levels:

$$\frac{d\phi^h}{d\Omega dE} = 1.49E^{-2.74}\frac{p}{\text{cm}^2\ \text{s sr GeV}} \tag{8}$$

for the hadronic background [63],

$$\frac{d\phi^e}{d\Omega dE} = 6.9\times10^{-2}E^{-3.3}\frac{e}{\text{cm}^2\ \text{s sr GeV}} \tag{9}$$

for the electron background [64], and

$$\frac{d\phi^\gamma_{diffuse}}{d\Omega dE} = 1.38\times10^{-6}E^{-2.1}\frac{\gamma}{\text{cm}^2\ \text{s sr GeV}} \tag{10}$$

for the diffuse extragalactic gamma emission, as extrapolated from EGRET data at lower energies [65].

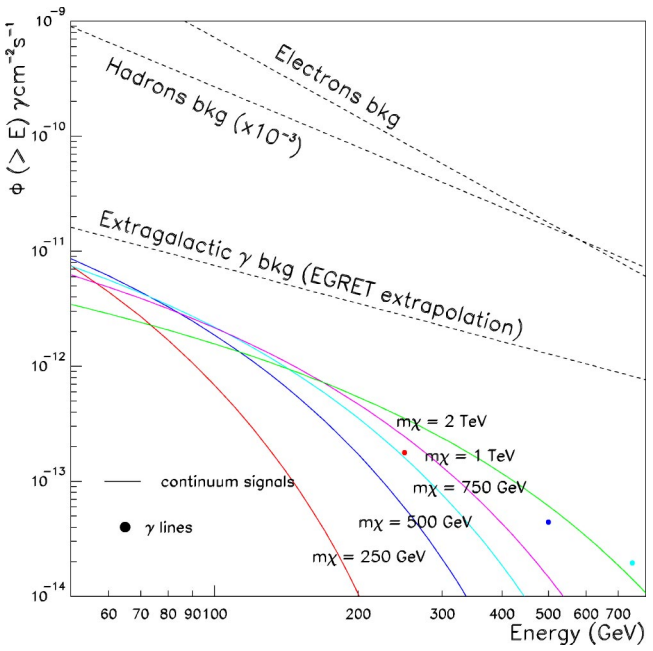

FIG. 7. Integrated spectra of photons from DM annihilation in M31 for different values of the neutralino mass, specified by the labels, computed assuming a Moore profile filled with a population of subgalactic halos unaffected by tides. Both the continuum emission (curves) and the γ-line contribution (filled dots) are shown. The relevant backgrounds (dashed lines) are shown for comparison.

The Galactic diffuse emission along M31 line of sight [12] turned out to be negligible with respect to the annihilation signal and has been neglected.

In Fig. 7 the various backgrounds (dashed lines) are compared to the integrated energy spectra of γ photons from DM annihilation in M31, computed assuming a Moore DM profile and a population of subhalos unaffected by tidal effects. The various curves refer to different neutralino masses, as specified by the labels. Filled dots represent the expected γ-line fluxes.

Figure 8 compares the expected integrated γ flux from M31 (dot-dashed curve) to the 5σ sensitivity curves for the large field of view array (upper line) and the Cerenkov telescope (lower line). The 5σ detection curves assume 1 year of data taking for the large field of view array and 20 days pointing for the Cerenkov telescope.

The results show that annihilation signals from M31, which are too faint for large field of view arrays, are well within reach of next generation Cerenkov telescopes.

B. Detectability of subhalos in our Galaxy

The only way of detecting signals from annihilation in Galactic subhalos is through blind searches since model predictions specify the subhalo distribution but not their precise spatial positions. In this regard, the use of a large field of view array has the advantage of collecting signals from a wide area of the sky, while ACTs would only allow us to survey a much smaller region.

To estimate the chances of detecting a γ-ray signal with either detectors we performed ideal observations with both instruments and computed the significance of an annihilation signal using Eq. (7).

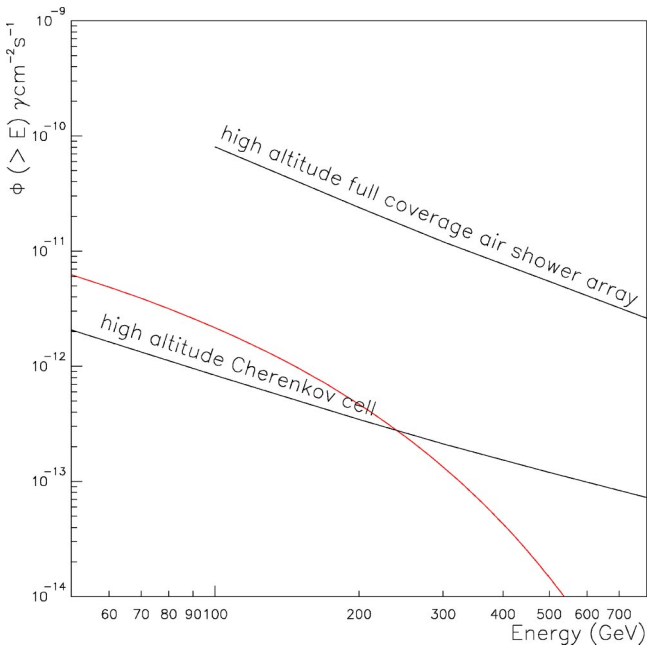

FIG. 8. 5σ sensitivity curves for a high altitude full coverage air shower array (upper line) and for a Cerenkov cell (lower line), computed using the parameters specified in the text. The curve shows the same flux from M31 displayed in Fig. 6 for the case of a neutralino mass of 1 TeV.

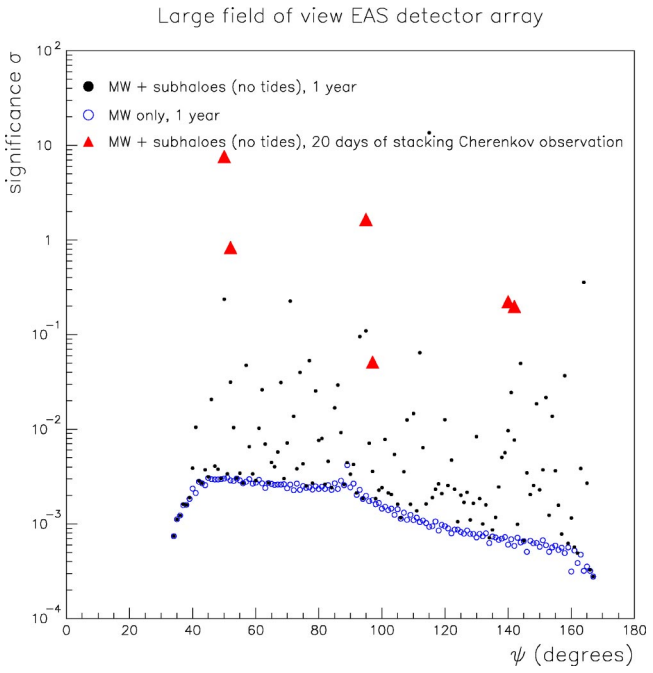

FIG. 9. Significance of the γ-ray signal from Galactic subhalos as a function of the angle of view from the GC, for a large field of view array (dots) and for a Cerenkov telescope (triangles). The considered subhalo distribution is not affected by any tidal effect.

We restrict our observations to all directions with $|b|<30°$ if $|l|<40°$ around the GC and $|b|<10°$ elsewhere provided that they are within a zenith angle of 30°. These constraints allow us to ignore the Galactic diffuse photon contribution to the background emission and the effects of the atmospheric depth.

For the case of a large field of view array we have chosen the ARGO experimental site (6.06 *h* E, 30.18° N) in Tibet and considered the case of a 365 days observation with a detector having an angular resolution of 1°. Each point in Fig. 9 represents the significance of a γ-ray signal detection in such an experiment, plotted as a function of ψ, the angle from the GC. Each filled dot accounts for the annihilation flux received from all Galactic subhalos with the same ψ that have entered the detector field of view during the observation. The Galactic signal in absence of subhalos is also plotted for reference (open dots). The significance detection level is very small at all ψ but in a couple of cases where a very nearby subhalo crosses the line of sight. The results show that it would be impossible, using a large field of view array, to identify the Galactic subhalo origin of any detected γ-ray flux.

For the case of an ACT we have chosen the VERITAS site (8.87 *h* W, 33° N) in Arizona. In this case we have considered the results of a 20 days ''stacking'' observation in which an instrument with an angular resolution of 0.1 degrees points toward different directions characterized by the same value of ψ. The results of this experiment are represented by the triangles in Fig. 9. Since each point represents a 20 days observation we have sampled only a few angles ψ. Although the significance of the ACT detections is higher than in the case of a large field of view array, the serendipitous nature of the γ-ray sources combined with the small extension of the surveyed area make it very hard to detect the annihilation signal from Galactic subhalos using Cerenkov telescopes.

We then conclude that only satellite borne experiments like GLAST will have the chance to detect γ-ray photons from Galactic subhalos and to study their spatial distribution [14].

VI. DISCUSSION AND CONCLUSIONS

In this work we have computed the expected γ-ray flux from DM annihilation in the nearest LG galaxies, under the assumption that the bulk of DM is constituted by neutralinos. Predicted fluxes depend on a number of assumptions like the shape of the DM halo density profiles, the possible existence and the distribution of a population of subgalactic halos, and the dynamical influence of SMBHs located at the halo centers. Uncertainties in these theoretical models that propagate into flux predictions have been evaluated by systematically exploring the space of the currently accepted model parameters.

It turns out that, in all cases considered, the fluxes from the Small and the Large Magellanic Clouds, M31 and M87 are well above the level of the γ-ray annihilation Galactic foreground. Uncertainties in the predicted Galactic emission are quite large (they vary by a factor ~ 100) and mainly result from the poorly known modeling of the DM substructures within our Galaxy. This scatter actually increases when considering more exotic possibilities that would further boost up the Galactic foreground like the existence of caustics in the DM distribution [66] or the presence of a population of

mini subhalos allowed by the very small cutoff mass in the CDM spectra [67]. Neutralino annihilation in subhalos contributes less to γ-ray flux from extragalactic sources, resulting in much smaller (by a factor of ~ 10) model uncertainties and more robust flux predictions.

In Sec. II we have assumed that the inner slope of the DM density profile $\rho(r) \propto r^{-\alpha}$ is in the range $1.0 < \alpha < 1.5$ following the indications of numerical experiments rather than using observational constraints. The reason was that current observations do not provide a self-consistent scenario. Indeed, recent determinations based on the x-ray properties of the intercluster medium seem to indicate a steep DM density profile $1.0 < \alpha < 2.0$, provided that clusters with disturbed x-ray surface brightness are removed from the sample [68,69]. On the other hand, the rotation curves measured in a sample of LSBs by [70] are consistent, on average, with a shallower density profile $\alpha = 0.2$. However, when the full extent of the rotation curves is taken into account rather than the inner region only, then the recovered density profiles lie between the NFW and the Moore ones [71]. Another study of high resolution $H\alpha$ rotation curves for dwarf and LSB [72] has ruled out neither profiles as steep as $\alpha = 1$ nor a constant density core. Finally, indications for shallow profiles ($\alpha = 0.52 \pm 0.3$) were found by combining stellar dynamics and strong lensing data in a sample of brightest cluster galaxies [73], and from microlensing events toward the GC ($\alpha = 0.4$, in the hypothesis that the MW halo is spherically symmetric [74]). However, estimates based on weak gravitational lensing in x-ray luminous clusters indicate a much steeper profile with $0.9 < \alpha < 1.6$ [75].

The previous examples show that the current observations neither support nor reject profiles as shallow as $\alpha = 0.5$ or 0. Therefore, while we regard the NFW and the Moore profiles as the most likely cases based on N-body results, we also want to keep an eye on the shallow profile case. For this purpose we have estimated the expected γ-ray flux from both M31 and LMC in the case of shallow profiles. If $\alpha = 0.5$ then the M31 flux is ~ 50 times smaller than in the NFW case and decreases by a further factor of 10 with a flat core $\alpha = 0$. Results for the LMC are very similar. Therefore, if the slope of the density profile would turn out to be as shallow as $\alpha = 0.5$ or more, then no ground-based experiments would have the chance of detecting extragalactic γ-ray annihilation fluxes.

In the hypothesis of both a NFW and a Moore DM density profile we have estimated the possibility of detecting the annihilation signals from Galactic subhalos and extragalactic sources using those ground based instruments sensitive enough to detect γ photons in the ~ 50 GeV–few TeV energy band, such as ACTs or large field of view arrays. We have found that the expected fluxes from Galactic subhalos are too faint to be detected by ground-based observatories. Their existence and distribution could instead be probed by next generation satellite borne experiments such as GLAST. On the other hand, ground-based experiments should be able to detect a few extragalactic objects such as LMC and M31. In particular, we have been focusing on M31 which turned out to be the brightest extragalactic object visible in most experimental sites. We have shown that next generation Čerenkov telescopes should be capable of revealing the γ-ray flux from M31 at a significance level $\simeq 5\sigma$ in a 20 days pointing observation. These results have been obtained using a quite conservative observational setup and theoretical modeling. Increasing the number of Čerenkov cells (as already planned for some future experiments) or the serendipitous superposition of a nearby Galactic subhalo would certainly increase the chance of detecting an annihilation signal along the M31 direction. The capability of detecting extragalactic signals is not shared by large shower arrays, which due to their lower sensitivity will not be able to detect such a faint source. It is worth stressing that the GC does remain the best place to consider for detecting DM annihilation signatures. Unfortunately, and unlike M31, it is not visible from the Northern Hemisphere where most of the ground-based detectors are (or will be) located.

Finally, it is worth stressing that our predictions assume that DM is made of neutralinos. However, the natural factorization of particle physics and cosmology in the problem addressed in this paper makes it straightforward to extend our approach to other kinds of weakly interacting DM candidates.

ACKNOWLEDGMENTS

We thank M. De Vincenzi, N. Fornengo, P. Gondolo, S. Matarrese and B. Moore for useful discussions and suggestions, and J. Navarro and E. Romano-Diaz for having provided numerical codes and graphic tools used in this work.

[1] D.N. Spergel *et al.*, Astrophys. J., Suppl. **148**, 175 (2003).
[2] J. Ellis *et al.*, Phys. Rev. D **62**, 075010 (2000).
[3] G. Jungman *et al.*, Phys. Rep. **267**, 195 (1996).
[4] N. Fornengo, Nucl. Phys. B (Proc. Suppl.) **95**, 221 (2001).
[5] J.L. Feng *et al.*, Phys. Lett. B **482**, 388 (2000).
[6] L. Bergström, Nucl. Phys. B (Proc. Suppl.) **81**, 22 (2000).
[7] J.L. Feng *et al.*, Phys. Rev. D **63**, 045024 (2001).
[8] A. Bottino *et al.*, Phys. Rev. D **58**, 123503 (1998).
[9] F. Donato *et al.*, Phys. Rev. D **62**, 043003 (2000).
[10] M. Urban *et al.*, Phys. Lett. B **293**, 149 (1992).
[11] V. Berezinsky *et al.*, Phys. Lett. B **325**, 136 (1994).
[12] L. Bergström *et al.*, Astropart. Phys. **9**, 137 (1998).
[13] C. Calcaneo-Roldan and B. Moore, Phys. Rev. D **62**, 123005 (2000).
[14] R. Aloisio, P. Blasi, and A. Olinto, astro-ph/0206036.
[15] P. Ullio *et al.*, Phys. Rev. D **66**, 123502 (2002).
[16] J. Taylor and J. Silk, Mon. Not. R. Astron. Soc. **339**, 505 (2003).
[17] L. Bergström, J. Edsjö, and P. Ullio, Phys. Rev. Lett. **87**, 251301 (2001).
[18] C. Tyler, Phys. Rev. D **66**, 023509 (2002).
[19] E.A. Baltz *et al.*, Phys. Rev. D **61**, 023514 (2000).

[20] A. Tasitsiomi, J. Gaskins, and A. Olinto, astro-ph/0307375.
[21] D. Fargion *et al.*, Astropart. Phys. **12**, 307 (2000).
[22] K. Griest and M. Kamionkowski, Phys. Rep. **333-334**, 167 (2000).
[23] B. Moore *et al.*, Phys. Rev. D **64**, 063508 (2001).
[24] F. Stoher *et al.*, Mon. Not. R. Astron. Soc. **345**, 1313 (2003).
[25] F. van den Bosch and R. Swaters, Mon. Not. R. Astron. Soc. **325**, 1017 (2001).
[26] A. Nusser and R. Sheth, Mon. Not. R. Astron. Soc. **303**, 685 (1999).
[27] K. Subramanian, Astrophys. J. **538**, 528 (2000).
[28] A. Dekel *et al.*, astro-ph/0205448.
[29] C. Power *et al.*, Mon. Not. R. Astron. Soc. **338**, 14 (2003).
[30] B. Moore *et al.*, Astrophys. J. Lett. **524**, L19 (1999).
[31] J.F. Navarro *et al.*, Astrophys. J. **490**, 493 (1997).
[32] M. Mateo, Annu. Rev. Astron. Astrophys. **36**, 435 (1998); http://www.ast.cam.ac.uk/~mike/local_members.html.
[33] V.R. Eke *et al.*, Astrophys. J. **554**, 114 (2001).
[34] D. McLaughlin, Astrophys. J. Lett. **512**, L9 (1999).
[35] V. Berezinsky *et al.*, Phys. Lett. B **294**, 221 (1992).
[36] P. Gondolo and J. Silk, Phys. Rev. Lett. **83**, 1719 (1999).
[37] P. Ullio, H. Zhao, and M. Kamionkowski, Phys. Rev. D **64**, 043504 (2001).
[38] M. Begelman *et al.*, Nature (London) **287**, 307 (1980).
[39] P.C. Peters, Phys. Rev. **136B**, 1224 (1964).
[40] D. Merritt and F. Cruz, Astrophys. J. Lett. **551**, L41 (2001).
[41] M. Milosavljević and D. Merritt, Astrophys. J. **563**, 34 (2001).
[42] M. Volonteri, P. Madau, and F. Haardt, Astrophys. J. **593**, 661 (2003).
[43] D. Merritt *et al.*, Phys. Rev. Lett. **88**, 191301 (2002).
[44] D. Merritt, L. Ferrarese, and C. Joseph, Science **293**, 1116 (2001).
[45] R. Genzel *et al.*, Mon. Not. R. Astron. Soc. **317**, 348 (2000).
[46] R.B. Tully and J.R. Fisher, Astron. Astrophys. **54**, 661 (1977).
[47] A.A. Klypin *et al.*, Astrophys. J. **522**, 82 (1999).
[48] E. Hayashi *et al.*, Astrophys. J. **584**, 541 (2003).
[49] N. Yoshida, A. Sokasian, and L. Hernquist, Astrophys. J. **1**, 591 (2003).
[50] S. Ghigna *et al.*, Astrophys. J. **544**, 616 (2000).
[51] P. Blasi and R.K. Sheth, Phys. Lett. B **486**, 233 (2000).
[52] L. Bergström, J. Edsjö, and P. Ullio, Phys. Rev. D **58**, 083507 (1998).
[53] A. Helmi, S. White, and V. Springel, Mon. Not. R. Astron. Soc. **339**, 834 (2003).
[54] A. Morselli *et al.*, in Proc. of the 32nd Rencontres de Moriond (1997).
[55] J. H. Buckley *et al.*, in Proc. of ''Towards a major atmospheric Čerenkov detector III'' (1994).
[56] V. Fonseca *et al.*, Nucl. Phys. B (Proc. Suppl.) **28A**, 409 (1992).
[57] F.A. Aharonian *et al.*, Astropart. Phys. **6**, 343 (1997).
[58] C. Baixeras *et al.*, Nucl. Phys. B (Proc. Suppl.) **114**, 247 (2003).
[59] T. C. Weekes *et al.*, in Proc. of the 25th ICRC, **5**, 173 (1997).
[60] M. De Vincenzi *et al.*, in Proc. of the 25th ICRC, **5**, 265 (1997).
[61] R. Atkins *et al.*, in Proc. of the 27th ICRC (2001).
[62] L. Pieri and E. Branchini, in Proc. of the 28th ICRC (2003), astro-ph/0307042.
[63] T. Gaisse *et al.*, in Proc. of the 27th ICRC (2001).
[64] M. S. Longair, *High Energy Astrophysics* (Cambridge University Press, Cambridge, England, 1992).
[65] P. Sreekumar *et al.*, Astrophys. J. **494**, 523 (1998).
[66] S.F. Shandarin and Ya.B. Zeldovich, Phys. Rev. Lett. **52**, 1488 (1984).
[67] V. Berezinsky *et al.*, Phys. Rev. D **68**, 103003 (2003).
[68] D.A. Buote, astro-ph/0310579.
[69] M.W. Bautz and J.S. Arabadjis, astro-ph/0303313.
[70] W.J.G. de Blok, A. Bosma, and S. McGaugh, Mon. Not. R. Astron. Soc. **340**, 657 (2003).
[71] E. Hayashi *et al.*, astro-ph/0310576.
[72] R.A. Swaters *et al.*, Astrophys. J. **583**, 732 (2003).
[73] D.J. Sand *et al.*, astro-ph/0309465.
[74] M.R. Merrifield, astro-ph/0310497.
[75] H. Dahle, astro-ph/0310549.